JOURNAL OF SOLID STATE CHEMISTRY **121,** 388–393 (1996)
ARTICLE NO. 0052

The Morphological Diagram of Spinels

Jacek Ziółkowski

Institute of Catalysis and Surface Chemistry, Polish Academy of Sciences, 30-237 Kraków, Poland

Received July 11, 1995; accepted October 19, 1995

Spinels exposing {100}, {110}, and {111} faces have been considered and their Curie–Wulff plots have been drawn, admitting that the relative $G\{hkl\}$ surface free energies may change in a wide range as a function of composition, inversion, and segregation degree. The normalized free surface energies are defined as $A = G\{100\}/G\{111\}$, $B = G\{110\}/G\{111\}$, and $C = G\{111\}/G\{111\} = 1 = \text{const}$. This made it possible to construct bidimensional morphological diagrams (morphology $= f(A, B)$ at $C = \text{const}$) in the exposed-face-type, solid-type, and exposure-percentage versions. Eleven morphological habits of grains have been identified, including {100}-cube, {110}-dodecahedron, {111}-octahedron, 14-hedron bordered with six {100}-squares and eight {111}-hexagons, 18-hedron, 20-hedron, and up to 26-hedra bordered with (i) 6 {100}-octagons, 12 {110}-rectangles, and 8 {111}-hexagons, (ii) 6 {100}-squares, 12 {110}-rectangles, and 8 {111}-triangles, or (iii) 6 {100}-squares, 12 {110}-octagons, and 8 {100}-triangles. The analysis is valid for all compounds crystallizing in the cubic system and preferentially exposing the three enumerated faces.

1. INTRODUCTION

Catalytic anisotropy (1–18) is now a well-known phenomenon in mild oxidation reactions. It involves the dependence of the reaction mechanism of a given reactant on the $\{hkl\}$ faces of the crystalline catalyst on which the transformation takes place. The most spectacular example of this phenomenon is the unique industrial catalyst for the selective oxidation of butane to maleic anhydride (14–17); it contains $(VO)_2P_2O_7$ prepared in a way that ensures the highly predominant exposure of the {100} face.

In the case of simple and complex oxides (oxysalts) we deal with the more or less anisotropic spatial distribution of atoms and consequently the metal–oxygen bond lengths and energies (19–22). As a result various "maps" of the $\{hkl\}$ faces of a given crystal differ in their composition, geometry, and local undersaturations. In view of this, differentiation of the molecule/$\{hkl\}$ face interactions becomes obvious. On the basis of such assumptions a number of theoretical models have been proposed (7, 9, 10, 23, 24), including the crystallochemical model of active sites (CMAS) established by the present author (9, 10), with which numerous anisotropic interactions in various reactant/catalyst systems have been explained (7–10, 16–18). An extension of CMAS is the crystallochemical model of solid surfaces (CMSS) (22), which offers the possibility of calculating the $\{hkl\}$ surface energies and the equilibrium morphology of crystals.

There are indications that the effect of catalytic anisotropy may be extended on the catalyst carriers, which may produce either the sites (areas) of the epitaxial growth of the conveniently oriented active phase or the growth of small especially active clusters (25–32).

So far, no systematic studies on the controlled morphology of crystals have been performed. Published data suggest that two approaches may be followed. One approach consists of preparing a convenient precursor which, after a fine decomposition or redox treatment, forms crystals of the desired shape, the same as that of the mother material. The above-mentioned plate-like V–P–O catalyst, prepared by decomposition of the layered hydrate, is a good example. However, a problem of long-term stability arises in this case. Another approach is to maintain the conditions of synthesis that ensure the equilibrium growth of crystals; presumably the change in chemical composition, segregation of dopants or other defects, and inversion in spinels should influence the crystal habit. The second case will be considered in the series of papers we intend to initiate with this work.

We decided to take spinels as model objects of studies on the crystal habit. For the purpose of this introductory work it will be enough to recall the following (33): Over 200 compounds with the composition AB_2X_4 (where X is the most frequently oxygen but is also S, Se, and Te) and innumerable solid solutions between them crystallize in the cubic $Fd3m$ spinel structure with eight formal molecules in the unit cell. The valence of A and B is most frequently 2–3, but can also be 4–2 or 6–1, e.g., $MgAl_2O_4$, $TiCo_2O_4$, and $MoNa_2O_4$. In this structure oxygens make almost ideal cubic close-packing. Cations are located in particular tetrahedral ( ) and octahedral [ ] holes of the oxygen sublattice. Three types of cation distribution are known: normal distribution $(A)[B_2]X_4$, inverse distribution $(B)[AB]X_4$, and intermediate distribution $(A_{1-z}B_z)[A_zB_{2-z}]X_4$, where z is the

0022-4596/96 $18.00

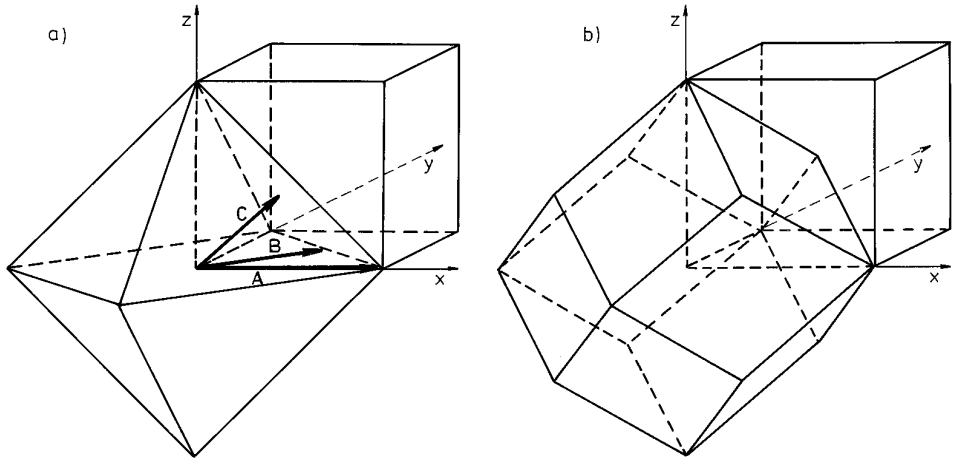

FIG. 1. The relative situation of solids: {100}-cube (1/8 is shown), {100}-dodecahedron, and {111}-octahedron, corresponding to the arbitrarily chosen normalized $C = 1$, $A = \sqrt{3}$, $B = \sqrt{2}\sqrt{3}/2$. Here, in terms of the Curie–Wulff plot, the {110}-solid makes an inner envelope with respect to the {100}-cube (b), and the {111}-octahedron is the inner envelope of all three solids (a).

so-called degree of inversion. As already mentioned, in addition to the binary spinels, more complex phases of this structure are known, such as $Mg_{1-x}Zn_xAl_2O_4$ and $MgAl_{2-x}Ga_xO_4$. In the latter phases, surface segregation of cations is expected. The variety of compositions, inversion degrees, and segregation extents permits one to believe that the surface energy of spinels (proportional to the energy of missing bonds) and consequently their habit may change in a wide range. The molecular aspects of the surface energy will be described in forthcoming papers in terms of CMSS. Here we present some geometrical considerations.

2. METHOD

We shall consider the grains of spinels remaining in both bulk and surface equilibrium with the environment. The first of these is obvious. As for the second, it seems relevant to recall that at a fixed temperature, pressure, and mass of a crystal the condition of the equilibrium crystal habit is that of minimum free surface energy,

$$\Sigma A_{hkl} G_{hkl} = \text{minimum}, \qquad [1]$$

where the sum is extended over all possible external $\{hkl\}$ faces, G_{hkl} and A_{hkl} being their free energies (per unit area) and areas, respectively. The equilibrium crystal habit can be derived from the Curie–Wulff plot (CWp) (34–36). In the CWp each vector from the origin to a point represents the direction of the normal to a particular face and the magnitude of the free energy of that particular face. The equilibrium shape of a crystal is the inner envelope of the CW planes drawn perpendicularly at the ends of vectors. Faces localized outside the inner envelope, but close to it, may exist as metastable faces.

It is known from the literature (37) that the spinels expose most frequently the {100}, {110}, and {111} faces, which means that these are the faces of the lowest $G\{hkl\}$. In this work the analysis of spinel morphology will be limited to these faces and all possible forms of crystals bordered with these faces will be searched for.

We shall use the normalized values A, B, and C of the surface energy defined as follows:

$$A = G\{100\}/G\{111\} \qquad [2a]$$

$$B = G\{110\}/G\{111\} \qquad [2b]$$

$$C = G\{111\}/G\{111\} = 1. \qquad [2c]$$

This way of energy normalization makes it possible to construct bidimensional morphological diagrams (as shown further in Figs. 2–4).

3. RESULTS

Let us consider first the solids bordered with only one type of $\{hkl\}$.

The {111}-solid is a regular octahedron. According to definition [2c], the faces are separated from the origin by $C = 1$, the corners by $\sqrt{3}$, and the edge lengths are $\sqrt{2}\sqrt{3}$.

The {100}-solid, according to [2a], is a cube of edge length $2A$, the corners being located at $A\sqrt{3}$ from the origin.

The {110}-solid is a dodecahedron with faces separated from the origin by B [2b]. Faces are rhombic with edges of $B\sqrt{2}\sqrt{3}/2$ and diagonals of $B\sqrt{2}$ and $2B$. Six corners

TABLE 1
Coexistence/Elimination Conditions for the Pairs of {100}-Cube, {110}-Dodecahedron, and {111} Octahedron Solids, in View of the Curie–Wulff Plot

Pair of bulks	Condition/conclusion		
	1	2	3
{111}, {100}	$A \le \sqrt{3}/3$ elim. {111} by {100}	$\sqrt{3}/3 < A < \sqrt{3}$ coexistence {111} + {100}	$\sqrt{3} \le A$ elim. {100} by {111}
{111}, {110}	$B \le \sqrt{2/3}$ elim. {111} by {110}	$\sqrt{2/3} < B < \sqrt{3/2}$ coexistence {111} + {110}	$\sqrt{3/2} \le B$ elim. {110} by {111}
{100}, {110}	$B \le A/\sqrt{2}$ elim. {100} by {110}	$A/\sqrt{2} < B < A\sqrt{2}$ coexistence {100} + {110}	$A\sqrt{2} \le B$ elim. {110} by {100}

of the dodecahedron are localized on the axes at $B\sqrt{2}$ from the origin; eight corners with the coordinates $(\pm x, \pm y, \pm z)$, $x = y = z = B\sqrt{2}$ are as far from the origin as $B\sqrt{3}/\sqrt{2}$.

For illustration, Fig. 1 has been constructed with $C = 1$, $B = \sqrt{2}\sqrt{3}/2$, and $A = \sqrt{3}$. With these values the {111}-octahedron is placed inside the {110}-dodecahedron and the later is placed inside the {100}-cube. Figure 1 may be considered a particular example of the CWp with a {111}-octahedron making the inner envelope.

Still keeping Fig. 1 in mind, one can easily show that with $A = \sqrt{3}/3$ (while again $C = 1$, $B = \sqrt{2}\sqrt{3}/2$) the {100}-cube would be placed inside both {111}- and {110}-solids. Consequently, as an inner envelope of CWp the {100}-cube would eliminate the {111} and {110} faces.

Analogous simple geometrical considerations enable us to determine all the conditions of coexistence/elimination of solid-bordering faces for the pairs of solids {111} + {100}, {111} + {110}, and {110} + {100}; e.g., for the pair {111} + {100} we deal with the {100}-cube for $A \le \sqrt{3}/3$, with a {111}-octahedron for $A \ge \sqrt{3}$, and with coexistence of both solids between these limits. All the results are summarized in Table 1.

An extension of the analogous analysis for all three types of {*hkl*}-solids is shown in Table 2 and in Fig. 2, the latter being the above-mentioned bidimensional morphological diagram of spinels, where the morphology is $f(A, B)$ at $C = 1 = \text{const}$.

Seven fields of coexistence/elimination of the {*hkl*} faces can be distinguished. In fields 1, 2, and 3 (including their boundary lines) only one type of face is exposed, {100}, {110}, or {111}, respectively. Fields 4, 5, and 6 (including their borders in common with 7) correspond to the exposure of pairs of faces, {100} + {110}, {110} + {111}, and

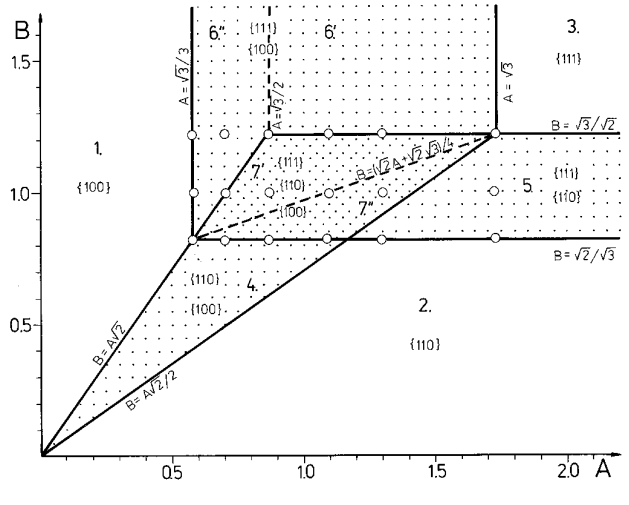

FIG. 2. The morphological diagram of spinels in the normalized surface energy coordinates; morphology = $f(A, B)$ at $C = 1$. The figure shows the "exposed-face-type version" of the diagram, i.e., the coexistence/elimination version. Fields are distinguished with arabic numbers. Circles correspond to the solids drawn in Fig. 3.

TABLE 2
Coexistence/Elimination Conditions for the {111}, {110}, and {100} Faces in View of the Curie–Wulff Plot

Field of diagram	Simultaneous conditions	Exposed faces	Polygon types
1	$A \le \sqrt{3}/3, B \ge A\sqrt{2}$	{100}	6× 4-gon
2	$B \le A\sqrt{2}/2, B \le \sqrt{2/3}$	{110}	12× 4-gon
3	$A \ge \sqrt{3}, B \ge \sqrt{3/2}$	{111}	8× 3-gon
4	$B < A\sqrt{2}, B > A\sqrt{2}/2,$ $B \le \sqrt{2/3}$	{100} {110}	6× 4-gon 12× 6-gon
5	$B < \sqrt{3/2}, B > \sqrt{2/3},$ $B \le A\sqrt{2}/2$	{110} {111}	12× 6-gon 8× 3-gon
6′	$A < \sqrt{3}, A > \sqrt{3}/2,$ $B \ge \sqrt{3/2}$	{100} {111}	6× 4-gon 8× 6-gon
border 6′/6″	$A = \sqrt{3}/2, B \ge \sqrt{3/2}$	{100} {111}	6× 4-gon 8× 3-gon
6″	$A > \sqrt{3}/3, A < \sqrt{3}/2,$ $B \ge A\sqrt{2}$	{100} {111}	6× 8-gon 8× 3-gon
7′	$B < \sqrt{3/2}, B < A\sqrt{2},$ $B > (A\sqrt{2} + \sqrt{2}\sqrt{3})/4 = X$	{100} {110} {111}	6× 8-gon 12× 4-gon 8× 6-gon
border 7′/7″	$B = X, \sqrt{3}/3 < A < \sqrt{3}$	{100} {110} {111}	6× 4-gon 12× 4-gon 8× 3-gon
7″	$B > A\sqrt{2}/2, B > \sqrt{2/3},$ $B < (A\sqrt{2} + \sqrt{2}\sqrt{3})/4 = X$	{100} {110} {111}	6× 4-gon 12× 8-gon 8× 3-gon

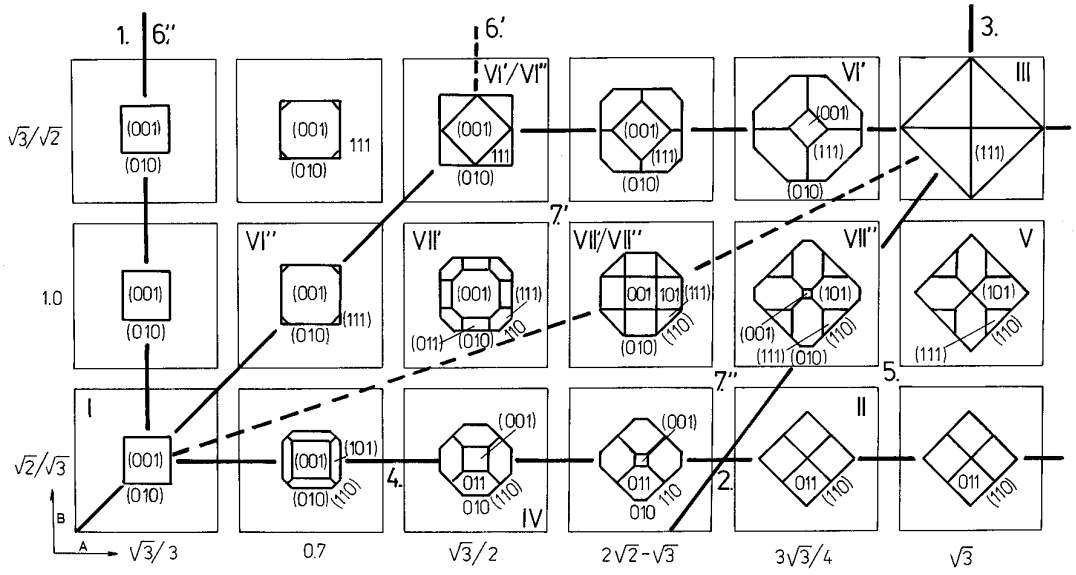

FIG. 3. The morphological diagram of spinels in the normalized surface energy coordinates; morphology = $f(A, B)$ at $C = 1$. The figure shows the ''solid-type version'' of the diagram, i.e., the x–y projections of solids as function of A and B. Fields and solid types are distinguished with arabic and roman numerals, respectively. Solids correspond to the circles in Fig. 2.

{100} + {111}, respectively. Finally, in field 7 exposure of all three faces is expected. Figure 2 will be called the ''face-type version'' of the morphological diagram.

However, if we take into account the types of polygons exposed, we have to divide field 6 into 6′ and 6″ and field 7 into 7′ and 7″, and moreover we must distinguish the borders 6′/6″ and 7′/7″. The types of polygons exposed are indicated in the last column of Table 2. In summary (in addition to seven fields of {*hkl*} coexistence/elimination) we must distinguish 11 morphological types (habits) of

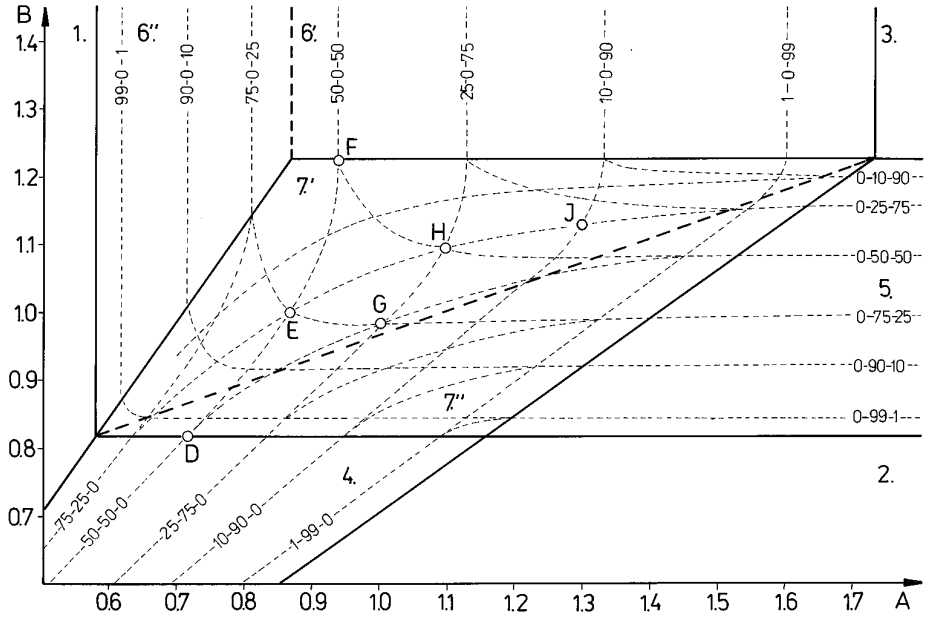

FIG. 4. The morphological diagram of spinels in the normalized surface energy coordinates; morphology = $f(A, B)$ at $C = 1$. The figure shows the ''exposition-percentage version'' of the diagram. X–Y–Z coordinates are ascribed to each line and to each point, expressing the percentage exposition of {100}, {110}, and {111} faces, respectively, e.g., E(50–25–25), H(25–25–50), J(10–25–65), G(25–50–25). The DEF line is the isopercentage line with respect to X ($X = 50$).

grains. The projections of these morphological forms are shown in Fig. 3, which may be called the ''solid-type version'' of the morphological diagram, in contrast to the face-type version shown in Fig. 2. Let us mention that a number of points have been marked with open circles in Fig. 2; the solids drawn in Fig. 3 correspond to the coordinates of these points.

If more than one face is exposed, a question about the extent (percentage) of exposure of each particular face arises. The relevant ''exposure-percentage version'' of the morphological diagram is shown in Fig. 4. A number of ''isopercentage lines'' are drawn in the figure, indexed with three numbers x–y–z expressing the percentage of exposure of {111}, {110}, and {100}, respectively; e.g., the line passing through DEF is the isopercentage line corresponding to $x = 50$, i.e., to the 50% impact of {100} in the external grain area. This line begins in field 4, where it is indexed as 50–50–0. This means obviously that {100} and {110} are equally exposed in this field and {111} is absent. The opposite end of the line, belonging to field 6, is marked 50–0–50, which means that {100} and {111} share equally and {110} is absent. A segment DF corresponds to 50% exposure of {100} and variable exposure of {110} and {111}. As may easily be deduced, the $x = 50\%$ line crosses in E the lines $y = 25\%$ and $z = 25\%$; the coordinates of E are thus E(50–25–25). Similarly we have G(25–50–25), H(25–25–50), and J(10–25–65), the last number for J resulting from the balance.

4. CONCLUSIONS

Simple and mixed AB_2X_4 spinels (where X = O, S, Se, Te and the valences of A–B may be 2–3, 4–2, or 6–1) belong to the huge family of compounds and solid solutions. They differ strongly in chemical composition, inversion degree, and segregation of dopants. Due to these characteristics, it has been supposed that their free energy $G\{hkl\}$ may vary in a wide range, influencing the equilibrium grain morphology. The most frequently exposed {100}, {110}, and {111} faces have been taken into account; their normalized G's have been introduced: $A = G\{100\}/G\{111\}$, $B = G\{110\}/G\{111\}$, and $C = G\{111\}/G\{111\} = 1 = \text{const}$. Curie–Wulff plots have been done. Due to the A–B–C normalization, bidimensional morphological diagrams of spinels have been constructed (morphology $= f(A, B)$ at $C = 1 = \text{const}$) in three versions: the exposed-face-type version (I), the solid-type version (II), and the exposition-percentage version (III).

—Version I enables us to distinguish seven fields where one, two, or three of the considered faces are exposed, the ranges of A and B being indicated in Table 2 and Fig. 2.

—Version II (Fig. 3) provides the projection of 11 kinds of habit ranging from the {100}-cube to the 26-hedra exposing all three considered faces.

—Version III (Fig. 4) makes it possible to read the percentage of each exposed face in the whole external areas of solids. One of the most complex solids (point G in Fig. 4, at $A = B = C = 1$) is the 26-hedron for which {100} and {111} make 25% and {110} makes 50% of its external area. Theoretical calculations of the surface energy, now in progress, indicate that the most probable habits are those belonging to fields 6′ and 7′.

The analysis is valid for all compounds crystallizing in the cubic system and preferentially exposing the three enumerated faces.

ACKNOWLEDGMENT

This work has been supported by the State Committee for Scientific Research, Warsaw, Poland (No. 2 P303 153 04).

REFERENCES

1. J. C. Volta, M. Forissier, F. Theobald, and T. P. Pham, *Faraday Discuss. Chem. Soc.* **72,** 225 (1981).
2. J. C. Volta and J. L. Portefaix, *Appl. Catal.* **18,** 1 (1985), and papers quoted therein.
3. J. M. Tatibouët and J. E. Germain, *J. Catal.* **72,** 375 (1981).
4. J. M. Tatibouët, J. E. Germain, and J. C. Volta, *J. Catal.* **82,** 240 (1993).
5. J. M. Tatibouët and J. E. Germain, *C. R. Acad. Sci. Paris C* **296,** 613 (1983).
6. J. Ziółkowski and J. Janas, *J. Catal.* **81,** 298 (1983).
7. J. Ziółkowski, *J. Catal.* **81,** 311 (1983).
8. J. Ziółkowski and M. Gąsior, *J. Catal.* **84,** 74 (1983).
9. J. Ziółkowski, *J. Catal.* **84,** 317 (1983).
10. J. Ziółkowski, *J. Catal.* **100,** 45 (1986).
11. M. Gąsior and T. Machej, *J. Catal.* **83,** 472 (1983).
12. M. Brückman, R. Grabowski, J. Haber, A. Mazurkiewicz, J. Słoczyński, and T. Wiltowski, *J. Catal.* **104,** 71 (1987).
13. S. T. Oyama, *Bull. Chem. Soc. Jpn.* **61,** 2585 (1988).
14. E. Bordes, *Catal. Today* **1,** 499 (1987).
15. E. Bordes, *Catal. Today* **3,** 163 (1988).
16. J. Ziółkowski, E. Bordes, and P. Courtine, *J. Catal.* **122,** 126 (1990).
17. J. Ziółkowski, E. Bordes, and P. Courtine, *J. Mol. Catal.* **84,** 307 (1993).
18. J. Ziółkowski and Y. Barbaux, *J. Mol. Catal.* **64,** 199 (1991).
19. J. Ziółkowski, *J. Solid State Chem.* **57,** 269 (1985).
20. J. Ziółkowski and L. Dziembaj, *J. Solid State Chem.* **57,** 291 (1985).
21. J. Ziółkowski, *J. Solid State Chem.* **61,** 343 (1986).
22. J. Ziółkowski, *Surface Sci.* **209,** 536 (1989).
23. A. Andersson, *J. Solid State Chem.* **42,** 263 (1982).
24. J. N. Allison and W. A. Goddard, *J. Catal.* **92,** 127 (1985).
25. A. Véjux and P. Courtine, *J. Solid State Chem.* **23,** 93 (1978).
26. A. Véjux and P. Courtine, *J. Solid State Chem.* **63,** 179 (1986).
27. A Véjux, E. Bordes and P. Courtine, *in* ''Proceedings, 9th European Chemistry of Interfaces Conference, Zakopane, Poland, 1986,'' *Mater. Sci. Forum* **25/26,** 475 (1988).
28. Y. Murakami, M. Yonomata, K. Mori, T. Ui, K. Suzuki, A. Miyamoto, and T. Hatori, *in* ''Preparation of Catalysts III'' (G. Poncelet, P. Grange, and P. A. Jacobs, Eds.), p. 531. Elsevier, Amsterdam (1983).
29. M. Gąsior, I. Gąsior, and B. Grzybowska, *Appl. Catal.* **10,** 87 (1984).

30. P. Courtine, *Amer. Chem. Soc. Symp. Ser.* **279,** 37 (1985).
31. T. Machej, B. Doumain, B. Yasse, and B. Delmon, *J. Chem. Soc. Faraday Trans.* **1,** 84 (1988).
32. R. Kozłowski, R. F. Petifer, and J. M. Thomas, *J. Phys. Chem.* **87,** 5176 (1983).
33. R. J. Hill, J. R. Craig, and G. V. Gibbs, *Phys. Chem. Minerals* **4,** 317 (1979).
34. P. Curie, *Bull. Soc. Mineral. France* **8,** 145 (1885).
35. G. Wulff, *Z. Krist. Mineral.* **34,** 449 (1901).
36. J. M. Blakley, ''Introduction to the Properties of Crystal Surfaces.'' Pergamon, Elmsford, NY, 1973.
37. C. Palache, H. Berman, and C. Frondel, (Dana's) ''The System of Mineralogy,'' Vol. I. Wiley, New York, 1944; Vol. II, Chapman and Hall, London, 1951.